NANO LETTERS

pubs.acs.org/NanoLett

New Nanostructured Li_2S/Silicon Rechargeable Battery with High Specific Energy

Yuan Yang,[†,§] Matthew T. McDowell,[†,§] Ariel Jackson,[†,§] Judy J. Cha,[†] Seung Sae Hong,[‡] and Yi Cui*[,†]

[†]Department of Materials Science and Engineering and , [‡]Department of Applied Physics, , and Stanford University, Stanford, California 94305

ABSTRACT Rechargeable lithium ion batteries are important energy storage devices; however, the specific energy of existing lithium ion batteries is still insufficient for many applications due to the limited specific charge capacity of the electrode materials. The recent development of sulfur/mesoporous carbon nanocomposite cathodes represents a particularly exciting advance, but in full battery cells, sulfur-based cathodes have to be paired with metallic lithium anodes as the lithium source, which can result in serious safety issues. Here we report a novel lithium metal-free battery consisting of a Li_2S/mesoporous carbon composite cathode and a silicon nanowire anode. This new battery yields a theoretical specific energy of 1550 Wh kg^{-1}, which is four times that of the theoretical specific energy of existing lithium-ion batteries based on $LiCoO_2$ cathodes and graphite anodes (~410 Wh kg^{-1}). The nanostructured design of both electrodes assists in overcoming the issues associated with using sulfur compounds and silicon in lithium-ion batteries, including poor electrical conductivity, significant structural changes, and volume expansion. We have experimentally realized an initial discharge specific energy of 630 Wh kg^{-1} based on the mass of the active electrode materials.

KEYWORDS Energy storage, lithium−sulfur battery, mesoporous carbon, silicon nanowires

Rechargeable batteries are critical power sources for mobile applications such as portable electronics and electric vehicles. However, the specific energy of existing lithium ion batteries is still insufficient for many applications due to the limited specific charge capacity of the electrode materials.[1−6] Despite significant progress in the development of high capacity anodes such as Si nanostructures,[7−11] the relatively low charge capacity of cathodes remains the limiting factor preventing higher energy density. Current cathode materials, such as those based on transition metal oxides and phosphates, have an inherent theoretical capacity limit of ~300 mAh g^{-1}, and a maximum practically usable capacity of only ~210 mAh g^{-1} has been reported.[3,6,12] The lithium/sulfur system, which during the redox process behaves according to the reaction $2Li + S \rightarrow Li_2S$, has the potential to overcome these capacity limitations. Although the system has an average voltage of ~2.2 V vs Li/Li^+ (about 60% of the voltage of conventional Li-ion batteries), the theoretical capacity of sulfur is 1672 mAh g^{-1}, which leads to a theoretical specific energy of ~2600 Wh kg^{-1} for the lithium/sulfur battery.[2,13] However, sulfur-based cathodes present a variety of problems, including low electronic conductivity, significant structural and volumetric changes during reaction, and dissolution of lithium polysulfides in the electrolyte. Much effort has been dedicated to improving this system, including the development of electrode coatings,[14] conductive additives,[6,15−17] and novel electrolytes.[18,19] Recently, cells utilizing a sulfur/mesoporous carbon nanocomposite exhibited capacity exceeding 1000 mAh g^{-1} and moderate cycle life.[6] Despite these advances, the use of elemental lithium as the anode in lithium/sulfur batteries remains a major problem due to safety concerns arising from the formation of lithium dendrites during cycling, which can penetrate the separator and lead to thermal runaway. Even though much research has been dedicated to solving this problem, an elemental lithium anode has not yet been commercialized for use in secondary batteries with a liquid electrolyte.[20]

One way to avoid this safety issue in the lithium/sulfur system is to use a high-capacity anode material other than elemental lithium while replacing sulfur in the cathode with its lithiated counterpart, lithium sulfide (Li_2S). Li_2S has a theoretical capacity of 1166 mAh g^{-1}, but its poor electronic conductivity restricts its actual capacity to much lower values that are not competitive with current commercial cathode materials.[21,22] Metal additives have been employed to enhance the conductivity of Li_2S-based cathodes with limited success. These experiments have mainly tested low-rate behavior[21,23] or have been based on very thin films.[22] The metal additives also alter the nature of the reaction, which results in a lower output voltage.[22,23] Moreover, a suitable anode with high capacity and low potential, which is crucial for achieving high specific energy, has not been demonstrated for a Li_2S-based cathode. In this study, we propose a novel nanostructured rechargeable battery consisting of a Li_2S/mesoporous carbon cathode and a silicon nanowire anode.

Figure 1a is a schematic showing the structure of this new Li_2S/Si battery. The cathode is comprised of a nanocompos-

* To whom correspondence should be addressed. E-mail: yicui@stanford.edu.

§ These authors contributed equally to this work.

Received for review: 02/10/2010
Published on Web: 02/25/2010

DOI: 10.1021/nl100504q | *Nano Lett.* **2010,** *10,* 1486–1491

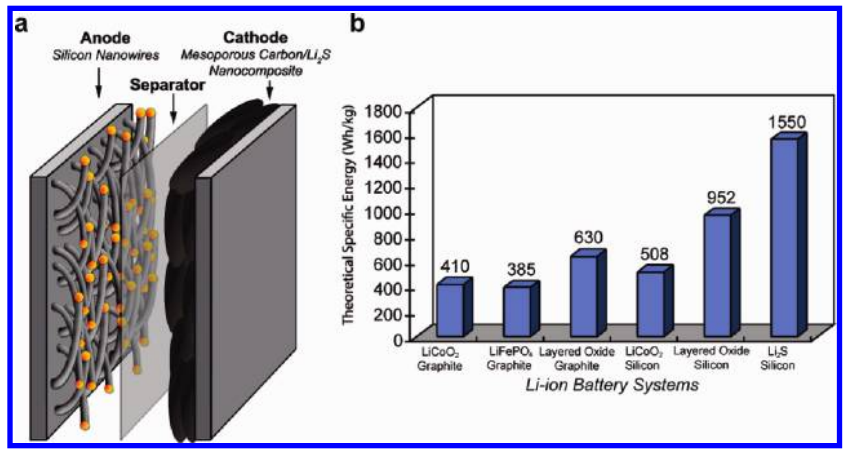

FIGURE 1. Schematic of the structure of a Li_2S/Si battery and specific energy comparison of different Li-ion battery systems. (a) Schematic diagram of battery structure; the cathode contains lithium sulfide (Li_2S) encapsulated within ordered mesoporous carbon, and the anode consists of silicon nanowires grown by the VLS mechanism. (b) Comparison of theoretical specific energy for different types of Li-ion batteries. The theoretical specific energy is calculated based on the theoretical capacities of the active materials in the electrodes and the average operating voltage of the battery. The Li_2S/Si battery has a much higher theoretical specific energy than other systems. It should be noted that the specific energy value for the $LiCoO_2$/graphite battery is based on a specific capacity value for $LiCoO_2$ of 155 mAh g^{-1}, which is a value that corresponds to extracting about half the lithium from the structure;[34] further extraction has been shown to compromise structural stability and cycle life.

ite in which Li_2S fills the pores of CMK-3 mesoporous carbon particles. CMK-3 carbon is made up of hexagonally arranged 7−8 nm thick carbon nanorods separated by 3−4 nm pores.[24] A previous study has shown that sulfur/CMK-3 composites exhibit good cycling behavior in lithium/sulfur batteries by partially confining readily dissolved lithium polysulfides formed during redox reactions within the mesoporous structure.[6] In addition, the interconnected carbon rods act as conductive pathways to provide electronic access to insulating Li_2S within the pores, while the submicrometer size of the carbon particles helps to shorten lithium diffusion paths. As a result, the problems associated with the slow kinetics of Li_2S-based cathodes can be solved. In the present case, the mesoporous carbon performs a similar role, although our new development is to use lithiated sulfur (Li_2S) as the starting active material in the cathode instead of sulfur. The anode shown in Figure 1a consists of silicon nanowires; silicon has a theoretical capacity of 4212 mAh g^{-1} and a low equilibrium potential of ~0.3 V versus Li/Li^+. Previous work from our group has shown that silicon nanowires can undergo the requisite 400% volume change upon insertion and extraction of lithium without pulverization or significant capacity fading over a number of cycles, which has plagued many previous silicon-based electrodes; furthermore, silicon anodes with a practical capacity of 2000 mAh g^{-1} and long cycle life have been fabricated.[7,8] In this report, we will demonstrate the successful coupling of silicon nanowire anodes with Li_2S-mesoporous carbon cathodes to attain high specific energy for the full battery cells.

Figure 1b compares the theoretical specific energy of our Li_2S/Si battery with other types of Li-ion batteries. The theoretical specific energy is based on the theoretical capacity of the active materials in both electrodes and their voltage difference (see Supporting Information for more details). The Li_2S/Si battery has a theoretical specific energy of 1550 Wh kg^{-1}, which is four times that of the $LiCoO_2$/graphite or $LiFePO_4$/graphite systems. This value is also 60% higher than the theoretical limit of mixed-layer oxide/silicon batteries.

To fabricate the Li_2S/mesoporous carbon nanocomposite cathode, ordered CMK-3 mesoporous carbon is first synthesized from a mesoporous silica template. CMK-3 has a uniform pore diameter of 3−4 nm, large pore volume (~1.0−1.5 cm^3 g^{-1}), and an interconnected pore structure that provides a conductive backbone for electron transfer. Sulfur is mixed with CMK-3 and made to diffuse into the pores by heating to 155 °C, where liquid sulfur has the lowest viscosity.[25] Since sulfur wets carbon well, the pores of mesoporous carbon are readily filled with sulfur due to the action of capillary forces. An electrode film is made from the sulfur/CMK-3 composite and then trapped sulfur is converted to lithium sulfide through a reaction with *n*-butyllithium. For the fabrication of the anode, silicon nanowires are grown on a stainless steel substrate using the well-known vapor−liquid−solid (VLS) method with silane gas as the precursor.[7,26] Next, an anode and a cathode with matched capacity are assembled in a pouch cell for electrochemical testing. The detailed fabrication process is described in the Supporting Information.

Transmission electron microscopy (TEM) was employed to analyze the composition and morphology of the as-prepared Li_2S/CMK-3 nanocomposite. Figure 2a shows a bright field image of a nanocomposite particle. The typical size of these particles is on the order of 0.5−1 μm. Selected area electron diffraction (Figure 2a inset) reveals no diffraction spots from the nanocomposite particle, indicating either that the lithiated sulfur is amorphous or the crystallite size is too small to generate diffraction spots due to the sub-5 nm pore size of the mesoporous carbon. Figure 2b,c displays

DOI: 10.1021/nl100504q | *Nano Lett.* **2010,** *10,* 1486–1491

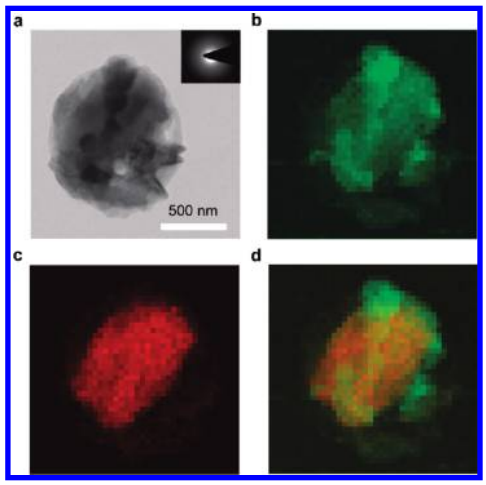

FIGURE 2. TEM image and elemental mapping of Li_2S/CMK-3 mesoporous carbon nanocomposite. (a) TEM image of a single Li_2S/CMK-3 mesoporous carbon nanocomposite particle. The inset shows the corresponding selected area electron diffraction pattern. (b,c) Elemental mapping of carbon (b) and sulfur (c) by energy-dispersive X-ray spectroscopy (EDS). (d) Overlay of carbon and sulfur elemental maps which shows uniform distribution of lithiated sulfur within the mesoporous carbon matrix. The orange color indicates the presence of both sulfur and carbon as orange is the result of mixing red (sulfur) and green (carbon) in a RG color scheme.

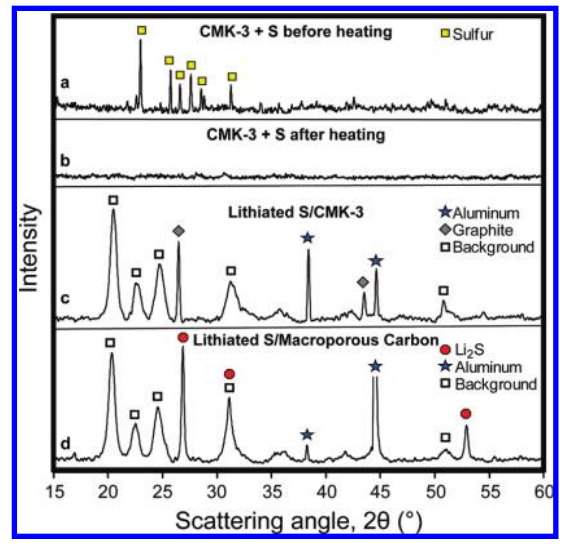

FIGURE 3. X-ray diffraction characterization of Li_2S/mesoporous carbon nanocomposite particles. (a,b) Scan of a mixture of sulfur and CMK-3 mesoporous carbon powder before heating (a) and after heating at 155 °C (b). (c) Scan of sulfur/CMK-3 mesoporous carbon nanocomposite lithiated by reaction with *n*-butyllithium and heated at 105 °C. The aluminum and graphite peaks are due to the carbon-coated aluminum foil substrate. (d) Scan of a sulfur/macroporous carbon nanocomposite lithiated by reaction with *n*-butyllithium and heated at 105 °C. The aluminum peaks are due to the aluminum foil substrate. The peaks labeled "Background" in c and d result from a protective cover used to prevent oxidation. Peaks are identified with the following symbols: yellow square, sulfur; blue star, aluminum; gray diamond, graphite; open square, background; red circle, Li_2S.

the corresponding elemental maps of carbon and sulfur obtained by energy-dispersive X-ray spectroscopy (EDS). Lithium is not included since it is a light element that cannot be identified with EDS. These elemental maps show that the element sulfur is distributed uniformly inside the mesoporous carbon matrix and that there is not a significant portion of sulfur on the surface, which is confirmed by superimposing the two elemental maps together (Figure 2d).

Scanning electron microscopy (SEM) characterization also supports this conclusion. No obvious change in the morphology or size of the sulfur/CMK-3 nanocomposite particles is observed after lithiation, which indicates formation of Li_2S within the pores of the CMK-3 particles (Figure S1 in the Supporting Information). However, the surface is visibly rougher, suggesting a small amount of Li_2S coating on the particles. This is likely due to the dissolution of sulfur in hexane during the lithiation process.

To further understand the composition and structure of the Li_2S/CMK-3 nanocomposite particles, X-ray diffraction (XRD) is used, as exhibited in Figure 3. Figure 3a shows a scan of a mixture of sulfur and CMK-3 particles before heating, and sulfur peaks are clearly present. These peaks disappear after heating because sulfur diffuses into the nanometer-sized pores of the mesoporous carbon (Figure 3b), which is in agreement with previous work.[6] After sulfur is lithiated by reaction with *n*-butyllithium, no peaks belonging to Li_2S or sulfur are present (Figure 3c). To verify that Li_2S is formed, sulfur was also lithiated inside macroporous carbon, which has larger pores (200−300 nm) than mesoporous carbon; these larger pores allow for the formation of Li_2S crystals that are large enough for detection with XRD.

Figure 3d shows a diffraction scan of lithiated sulfur inside macroporous carbon, and as expected, Li_2S peaks are clearly evident. We believe that Li_2S is also present in lithiated sulfur/CMK-3 mesoporous carbon, but the sub-5 nm pores in the mesoporous carbon diminish the Li_2S diffraction peaks by limiting the crystallite size to a few nanometers. These results are consistent with TEM and SEM observations and also suggest that Li_2S is trapped inside the mesoporous carbon after lithiation.

To understand the electrochemical behavior of the Li_2S/mesoporous carbon cathode, half-cells with lithium foil as the counter electrode were tested. Figure 4a shows the voltage profile of a Li_2S/CMK-3 mesoporous carbon cathode half-cell. The first discharge capacity of the Li_2S/mesoporous carbon cathode reaches 573 mAh g^{-1} (all capacity calculations are based on the mass of Li_2S, not sulfur). As a result, about 50% of the theoretical capacity is achieved, which is better than values in some reports of lithium/sulfur batteries.[5,15,27,28] Figure S2 in the Supporting Information displays the first cycle voltage profiles of this Li_2S/mesoporous carbon cathode and a cathode made from Li_2S powder (~500 nm in size), both of which contain the same fraction of Li_2S. Comparison of the charge profiles of the two electrodes reveals a similar electrochemical signature, which further indicates that the starting product in the CMK-3 composite electrode is Li_2S. In addition, the Li_2S/mesoporous carbon electrode exhib-

DOI: 10.1021/nl100504q | *Nano Lett.* **2010,** *10,* 1486–1491

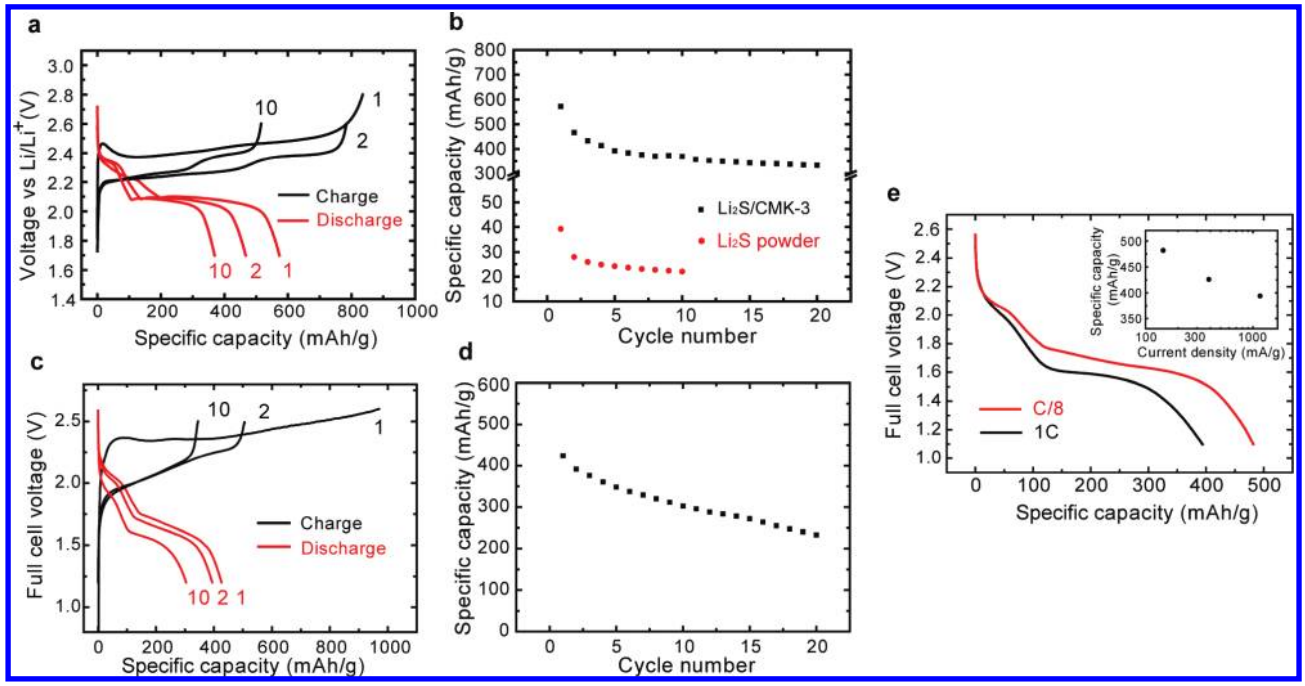

FIGURE 4. Electrochemical tests of Li_2S/Li half-cells and Li_2S/Si full cells. All specific capacity values are given with respect to the mass of Li_2S. (a,b) Voltage profile (a) and specific discharge capacity with cycling (b) of a Li_2S/CMK-3 mesoporous carbon nanocomposite half-cell containing a lithium counter electrode. The current rate is C/8 (146 mA g^{-1}) and the voltage range is 1.7−2.8 V for the first cycle and 1.7−2.6 V for following cycles. The specific discharge capacity with cycling of a Li_2S commercial powder half-cell is also shown for comparison in (b). (c,d) Voltage profile (c) and specific discharge capacity with cycling (d) of a full battery cell with a Li_2S/CMK-3 mesoporous carbon nanocomposite cathode and a silicon nanowire anode. The current rate is C/3 (389 mA g^{-1}) and the voltage range for the full cell is 1.2−2.6 V for the first cycle and 1.2−2.5 V for following cycles. (e) First discharge voltage profiles of full battery cells with Li_2S/CMK-3 mesoporous carbon nanocomposite cathodes and silicon nanowire anodes at rates of 1C (1166 mA g^{-1}) and C/8 (146 mA g^{-1}). The inset in (e) is a plot of the first discharge specific capacity of full cells operating at various current rates.

its an order of magnitude higher capacity than the Li_2S powder electrode, which demonstrates the significantly improved kinetics resulting from the rational design of the Li_2S/mesoporous carbon particles.

It is evident from the voltage profile shown in Figure 4a that the first charge is different than subsequent charges. The first charge voltage is higher and shows a clear phase nucleation barrier at the onset of charging, while the voltage profile of the following charge/discharge cycles is similar to that of typical lithium/sulfur batteries as reported in other works; the upper plateau corresponds to the redox reaction of high-order polysulfides (Li_2S_x, $4 \leq x \leq 8$), and the lower plateau is due to the reaction of low-order sulfides (Li_2S_2 and Li_2S).[13,29] These observations might be attributed to the fact that before cycling, the only electrochemically active phase in the cathode is Li_2S, which is different from that in lithium/sulfur batteries. At the beginning of charge in lithium/sulfur batteries, the cathode contains a mixture of Li_2S and lithium polysulfides; these polysulfides improve the kinetic behavior of the cathode. Nevertheless, the difference in potential of only ~200 mV between the first charge and subsequent charges, as shown in Figure 4a, further demonstrates the substantially enhanced kinetics of Li_2S resulting from its incorporation in the mesoporous carbon nanocomposite. Figure 4b shows the discharge capacity over a number of cycles for the Li_2S cathode. The first discharge capacity is 573 mAh g^{-1}, and the capacity is stabilized after five cycles. We believe that further improvements in cycling behavior and capacity retention can be attained through optimization of the system, including utilization of better electrolytes and surface modifications of the electrodes.

To study the effect of the structure and morphology of the Li_2S/carbon nanocomposite on resulting electrochemical performance, it is useful to compare data from Li_2S/CMK-3 mesoporous carbon and Li_2S/macroporous carbon tested in half-cell configurations. The process of lithiation and battery fabrication is the same for both cases. For the Li_2S/macroporous carbon composite, a capacity of 150 mAh g^{-1} is obtained (Figures S3 and S4 in the Supporting Information). The initial charging voltage is higher than in Li_2S/CMK-3 half-cells, suggesting a larger overpotential. The lower capacity and higher overpotential of Li_2S/macroporous carbon indicates the importance of the size, morphology, and structure of porous carbon on the corresponding electrochemical performance of the composite. Small pore size with strong confinement is important for minimizing charge transport distances and thus achieving good performance.

Since the key purpose of incorporating Li_2S instead of sulfur as the active cathode material is to avoid using potentially unsafe lithium metal anodes, full cells with silicon nanowire anodes were fabricated. This full cell configuration can also demonstrate that the source of lithium during

DOI: 10.1021/nl100504q | *Nano Lett.* **2010,** *10,* 1486–1491

charge and discharge is the Li_2S cathode since there is no other lithium in the cell. In contrast, the source of lithium in the Li_2S/Li half-cells is unclear since a lithium foil counter electrode is present. As the first step, silicon nanowire electrodes were characterized and tested in a half-cell configuration with lithium foil counter electrodes and the same electrolyte utilized in the Li_2S/Li half-cells; the capacity reached ~3000 mAh g^{-1} with moderate cycle life (Figure S5 in the Supporting Information). Next, fresh silicon nanowire anodes prepared under identical conditions were assembled together with Li_2S/CMK-3 cathodes for full cell electrochemical tests. Figure 4c shows the voltage profiles of the first, second, and tenth charge and discharge cycles for a Li_2S/Si battery at a rate of C/3, which corresponds to 389 mA g^{-1} with respect to Li_2S. The average discharge voltage of the Li_2S/Si full cell is ~1.7 V since the silicon anode has an average discharge potential of ~0.4 V versus Li/Li^+, and the first discharge capacity reaches 423 mAh g^{-1}. The corresponding capacity retention with cycling for the Li_2S/Si battery is shown in Figure 4d. Even at a 1C current rate (1166 mA g^{-1}), the initial capacity remains similar (394 mAh g^{-1}, Figure 4e). The corresponding current density per unit area for a rate of 1C is about 1.5 mA cm^{-2}, which is more than 20 times greater than the current density in previous reports.[21,22] The discharge capacity can be further enhanced by lowering the discharge current. At C/8 (146 mA g^{-1}), the first discharge capacity increases to 482 mAh g^{-1} (Figure 4e), which results in an initial specific energy of 630 Wh kg^{-1} for the full cell considering active materials only. If the masses of all electrode additives (CMK-3, PVDF, Super P conductive carbon) are considered, the initial specific energy is calculated to be 349 Wh kg^{-1}, which is similar to that of commercial Li-ion batteries (335 Wh kg^{-1}). With further optimization of this battery, however, we project that the specific energy could reach ~600 Wh kg^{-1} considering the total electrode mass (see Supporting Information for calculation details). It should be noted that since a 1C current rate for Li_2S is about six to eight times that of layered oxides and phosphates (140−200 mA g^{-1}), a rate of C/8 for a Li_2S-based cathode would provide adequate power for many applications.

From comparison of Figure 4 panels b and d, the specific capacity of the Li_2S/Si full cell decays faster than the specific capacity of the Li_2S/Li half-cell. This could be caused by the following factors: (1) In full cells, there is a limited supply of Li ions, which can be irreversibly lost in side reactions. In half-cells, Li ions that would be lost in a full cell configuration can be replenished by the Li metal counter electrode, which is a virtually unlimited source of Li ions. (2) The voltage of each electrode is not separately controlled in full cells. The deep discharge or overcharge of Li_2S or silicon is detrimental to cycling performance, and this might occur during cycling since we only control the voltage of the full cell. Although the capacity decay from the first to the 20th cycle from our proof-of-concept Li_2S/Si battery is better or comparable to many other reports on Li_2S or sulfur−lithium batteries,[22,23,27,30−33] more research is required to overcome these issues and compete with well-developed Li-ion battery systems. In addition to these concerns, the volumetric energy density of our current cell is not as high as the $LiCoO_2$/graphite system, even though the theoretical volumetric energy density of the Li_2S/Si system is about twice that of the $LiCoO_2$/graphite system (See Table S3 in the Supporting Information).

In summary, we demonstrate a new type of rechargeable Li-ion battery containing Li_2S and silicon as the active materials in the cathode and anode, respectively. Li_2S is made electrochemically active by incorporating it within the pores of CMK-3 mesoporous carbon in the cathode. Silicon nanowire anodes are demonstrated to be ideal for this battery system due to their high capacity, low reaction potential, and moderate cycle life. The theoretical specific energy of this new battery is four times that of state-of-the-art battery technology, and cells with 70% higher first discharge specific energy than the commercial $LiCoO_2$/graphite system have been fabricated. Additionally, this new battery system avoids the intrinsic safety issues associated with the use of lithium metal in previous lithium/sulfur batteries. The development of this novel battery system will have a significant impact on applications that require high specific energy, such as batteries for electric vehicles and portable electronics.

Acknowledgment. We would like to thank Dr. Fabio La Mantia at Stanford University for helpful discussions. Y.C. acknowledges support from the King Abdullah University of Science and Technology (KAUST) Investigator Award (No. KUS-l1-001-12) and MDV Innovators Award. Y.Y. acknowledges support from a Stanford Graduate Fellowship. M.T.M. acknowledges support from a Stanford Graduate Fellowship and a National Defense Science and Engineering Graduate Fellowship.

Supporting Information Available. Additional figures and tables depicting experimental results. This material is available free of charge via the Internet at http://pubs.acs.org.

REFERENCES AND NOTES

(1) Tarascon, J. M.; Armand, M. *Nature* **2001**, *414* (6861), 359–367.
(2) Mikhaylik, Y. V.; Akridge, J. R. *J. Electrochem. Soc.* **2004**, *151* (11), A1969–A1976.
(3) Whittingham, M. S. *Chem. Rev.* **2004**, *104* (10), 4271–4301.
(4) Arico, A. S.; Bruce, P.; Scrosati, B.; Tarascon, J. M.; Van Schalkwijk, W. *Nat. Mater.* **2005**, *4* (5), 366–377.
(5) Sun, J.; Huang, Y. Q.; Wang, W. K.; Yu, Z. B.; Wang, A. B.; Yuan, K. G. *Electrochim. Acta* **2008**, *53* (24), 7084–7088.
(6) Ji, X. L.; Lee, K. T.; Nazar, L. F. *Nat. Mater.* **2009**, *8* (6), 500–506.
(7) Chan, C. K.; Peng, H. L.; Liu, G.; McIlwrath, K.; Zhang, X. F.; Huggins, R. A.; Cui, Y. *Nat. Nanotechnol.* **2008**, *3* (1), 31–35.
(8) Cui, L. F.; Ruffo, R.; Chan, C. K.; Peng, H. L.; Cui, Y. *Nano Lett.* **2009**, *9* (1), 491–495.
(9) Cui, L. F.; Yang, Y.; Hsu, C. M.; Cui, Y. *Nano Lett.* **2009**, *9* (9), 3370–3374.

DOI: 10.1021/nl100504q | *Nano Lett.* **2010,** *10,* 1486–1491

(10) Esmanski, A.; Ozin, G. A. *Adv. Funct. Mater.* **2009**, *19* (12), 1999–2010.
(11) Park, M.-H.; Kim, M. G.; Joo, J.; Kim, K.; Kim, J.; Ahn, S.; Cui, Y.; Cho, J. *Nano Lett.* **2009**, *9* (11), 3844–3847.
(12) Sun, Y. K.; Myung, S. T.; Park, B. C.; Prakash, J.; Belharouak, I.; Amine, K. *Nat. Mater.* **2009**, *8* (4), 320–324.
(13) Joongpyo, S.; Striebel, K. A.; Cairns, E. J. *J. Electrochem. Soc.* **2002**, *149* (10), A1321–5.
(14) Choi, Y. J.; Chung, Y. D.; Baek, C. Y.; Kim, K. W.; Ahn, H. J.; Ahn, J. H. *J. Power Sources* **2008**, *184* (2), 548–552.
(15) Lai, C.; Gao, X. P.; Zhang, B.; Yan, T. Y.; Zhou, Z. *J. Phys. Chem. C* **2009**, *113* (11), 4712–4716.
(16) Wang, J. L.; Yang, J.; Xie, J. Y.; Xu, N. X. *Adv. Mater.* **2002**, *14* (13−14), 963+.
(17) Yuan, L. X.; Yuan, H. P.; Qiu, X. P.; Chen, L. Q.; Zhu, W. T. *J. Power Sources* **2009**, *189* (2), 1141–1146.
(18) Shin, J. H.; Cairns, E. J. *J. Power Sources* **2008***177* (2), 537 545.
(19) Yuan, L. X.; Feng, J. K.; Ai, X. P.; Cao, Y. L.; Chen, S. L.; Yang, H. X. *Electrochem. Commun.* **2006**, *8* (4), 610–614.
(20) Nishikawa, K.; Fukunaka, Y.; Sakka, T.; Ogata, Y. H.; Selman, J. R. *J. Electrochem. Soc.* **2007**, *154* (10), A943–A948.
(21) Hayashi, A.; Ohtsubo, R.; Ohtomo, T.; Mizuno, F.; Tatsumisago, M. *J. Power Sources* **2008**, *183* (1), 422–426.
(22) Zhou, Y. N.; Wu, C. L.; Zhang, H.; Wu, X. J.; Fu, Z. W. *Electrochim. Acta* **2007**, *52* (9), 3130–3136.
(23) Obrovac, M. N.; Dahn, J. R. *Electrochem. Solid State Lett.* **2002**, *5* (4), A70–A73.
(24) Jun, S.; Joo, S. H.; Ryoo, R.; Kruk, M.; Jaroniec, M.; Liu, Z.; Ohsuna, T.; Terasaki, O. *J. Am. Chem. Soc.* **2000**, *122* (43), 10712–10713.
(25) Miessler, G. L.; Tarr, D. A. *Inorganic Chemistry*; Prentice Hall: New Jersey, 1998.
(26) Cui, Y.; Lieber, C. M. *Science* **2001**, *291* (5505), 851–853.
(27) Marmorstein, D.; Yu, T. H.; Striebel, K. A.; McLarnon, F. R.; Hou, J.; Cairns, E. J. *J. Power Sources* **2000**, *89* (2), 219–226.
(28) Han, S. C.; Song, M. S.; Lee, H.; Kim, H. S.; Ahn, H. J.; Lee, J. Y. *J. Electrochem. Soc.* **2003**, *150* (7), A889–A893.
(29) Yamin, H.; Gorenshtein, A.; Penciner, J.; Sternberg, Y.; Peled, E. *J. Electrochem. Soc.* **1988**, *135* (5), 1045–1048.
(30) Jeon, B. H.; Yeon, J. H.; Kim, K. M.; Chung, I. J. *J. Power Sources* **2002**, *109* (1), 89–97.
(31) Jeong, S. S.; Lim, Y.; Choi, Y. J.; Cho, G. B.; Kim, K. W.; Ahn, H. J.; Cho, K. K. *J. Power Sources* **2007**, *174* (2), 745–750.
(32) Lee, Y. M.; Choi, N. S.; Park, J. H.; Park, J. K. *J. Power Sources* **2003**, *119*, 964–972.
(33) Sun, M. M.; Zhang, S. C.; Jiang, T.; Zhang, L.; Yu, J. H. *Electrochem. Commun.* **2008**, *10* (12), 1819–1822.
(34) Linden, D.; Reddy, T. B. Handbook of Batteries. In *Handbook of Batteries*, 3rd ed.; McGraw-Hill: New York, 2002; pp 35.1−35.94.

DOI: 10.1021/nl100504q | *Nano Lett.* **2010,** *10,* 1486--1491